IOP PUBLISHING JOURNAL OF PHYSICS G: NUCLEAR AND PARTICLE PHYSICS

J. Phys. G: Nucl. Part. Phys. **34** (2007) 1935–1953 doi:10.1088/0954-3899/34/9/007

Systematic study of fusion barriers

Ning Wang[1], **Zhuxia Li**[2] **and Werner Scheid**[1]

[1] Institute for Theoretical Physics at Justus-Liebig-University, D-35392 Giessen, Germany
[2] China Institute of Atomic Energy, Beijing 102413, People's Republic of China

E-mail: Ning.Wang@theo.physik.uni-giessen.de

Received 26 February 2007
Published 31 July 2007
Online at stacks.iop.org/JPhysG/34/1935

Abstract

A possible method is proposed for extracting fusion barriers from measured fusion excitation functions. The obtained fusion barrier distributions are in good agreement with those determined by the $d^2(E\sigma_{fus})/dE^2$ method. The characteristics of the fusion barrier distributions, such as the mean barrier heights, the full widths at half maximum as well as the radii of the barriers, are studied systematically. A systematic comparison between the characteristics of the fusion barrier distributions determined by the proposed method and those of empirical barrier distributions based on the nucleus–nucleus potential calculated with Skyrme energy-density functional together with extended Thomas–Fermi approach has been performed for 120 fusion reactions. A nice agreement between them is found. Simultaneously, the influence of the static deformation and the deformation due to excitation of the reaction partners on the reduction of the fusion barriers was investigated for a series of reactions. From the investigation of the deviation of the calculated fusion excitation functions based on different Skyrme interactions from the experimental data, we find that the nucleus–nucleus potential obtained with SkM* can provide a better description of the fusion cross sections at energies near and above the barrier systematically.

(Some figures in this article are in colour only in the electronic version)

1. Introduction

The study of fusion barriers in heavy-ion fusion reactions has attracted a lot of attention [1–12], since the fusion barriers have close relations with nucleus–nucleus interaction and fusion mechanism, and furthermore, the study of fusion barriers is quite helpful for synthesis of super-heavy nuclei and understanding of nuclear structure effects. It is of great importance to propose and/or check theoretical nucleus–nucleus interaction and to explore the global features of the fusion barriers through a systematic study of the fusion barriers based on a

large number of measured experimental data of fusion reactions. As the fusion barriers could not be measured directly in experiments, to extract and analyze the fusion barriers based on the directly measured fusion excitation functions is essentially necessary for establishing a reliable theoretical model for describing fusion reactions. Then, combining the theoretical nucleus–nucleus interaction and the extracted fusion barriers, the fusion mechanism such as a reduction of the fusion barriers due to the deformation of the reaction partners and the influence of nuclear potentials on the fusion cross sections can be explored.

With the precisely measured fusion cross section, the fusion barrier and its characteristics such as the height and the position of the barrier could be extracted. But it is well known that the simple one-dimensional barrier penetration cannot describe the fusion cross sections of heavy systems at sub-barrier energies satisfactorily. Therefore, a barrier distribution is introduced to take into account the coupling between the relative motion of the two nuclei and other degrees of freedom [2]. It was shown in [3–5] that the distribution of the fusion barrier heights could be extracted directly from a fusion excitation function using the second derivative of the product of cross section $\sigma_{\rm fus}$ multiplied by the energy E. The differentiation $\mathrm{d}^2(E\sigma_{\rm fus})/\mathrm{d}E^2$ is performed using the point-difference approximation [4, 5]. This method requires very high precision and small well-determined energy steps of the measured cross sections. Thus, the fusion barriers of a number of reactions measured before cannot be analyzed with the method because of the relatively low precision and large energy steps. Furthermore, since the statistical error of the fusion barrier distribution associated with the double differentiation of $E\sigma_{\rm fus}$ is proportional to E, it is difficult to precisely determine the over-barrier part of the distribution with this method.

In addition to the double differentiation method, there still exist some other methods for obtaining the information about the fusion barriers based on the measured fusion excitation functions by combining theoretical formulae of the fusion cross section. In [8], a large number of measured fusion excitation functions, at energies above the average fusion barriers, have been fitted by using the Woods-Saxon form of the nuclear potential in a barrier passing model of fusion. The data above the barrier region were fitted by using the modified Wong formula in which the dependence of the fusion radius on the incident energy is taken into account together with the Woods-Saxon potential with three parameters to be determined. In [12], a simple formula for the cross section for overcoming the potential barrier based on the classical expression $\sigma_{\rm fus}(E) = \pi R_{\rm fus}^2(1 - B/E)$ was proposed, assuming a single Gaussian distribution of the barrier heights. The parameters of the Gaussian distribution were obtained by fitting the measured fusion excitation function. The advantage of this method is that it does not require a very high precision of the measured fusion excitation function compared with the $\mathrm{d}^2(E\sigma_{\rm fus})/\mathrm{d}E^2$ method and thus a lot of experimental data obtained before with a little lower precision can also be analyzed for obtaining helpful information about the fusion barriers. Nevertheless, the shape of a single Gaussian distribution of barrier is not consistent with the barrier distribution determined by the $\mathrm{d}^2(E\sigma_{\rm fus})/\mathrm{d}E^2$ method as it has been found that the fusion barrier distributions by this method are not symmetric for most fusion reactions. It means that multi-Gaussian functions for describing the fusion barrier distribution are needed.

In the first part of this work, we will propose a method to obtain the information about the fusion barriers from the measured fusion excitation functions by combining Wong's formula [1] for the fusion cross section with the fusion barrier distribution which is a superposition of a set of Gaussian functions with fitting parameters. The obtained results will be compared with those of the methods mentioned above.

It is known that the fusion barrier distributions are well explained with the fusion-coupled channel model [7] with a certain nucleus–nucleus potential. However there still exist some difficulties to find a potential by which the available experimental data of the

fusion reactions from light to heavy systems can be well reproduced systematically and thus the fusion cross sections of unmeasured reactions can be predicted reliably. For describing the fusion reactions systematically, we proposed a parametrization of the empirical barrier distribution in [14] based on the fusion barrier calculated with the Skyrme energy density functional. By combining the empirical distribution for fusion barrier heights with the Wong formula, the fusion cross sections for reaction systems can be calculated. In this work we will make a systematic comparison of the parametrization of the empirical fusion barrier distribution given in [14] with the fusion barrier determined from the measured experimental data. In addition, for understanding the physics behind the extracted and the empirical fusion barrier distributions, the influence of the nuclear deformation on the reduction of the fusion barriers will be investigated with the same energy-density functional for a series of fusion reactions induced by ^{16}O.

The paper is organized as follows: in section 2, the detailed procedure for extracting the fusion barriers is introduced and some results are presented simultaneously. In section 3, theoretical analysis on the fusion barriers is discussed. Finally, the summary and discussion are given in section 4.

2. Fitting procedure and obtained fusion barriers

Taking into account the multi-dimensional character [15] of the realistic barrier, the fusion excitation function is given by

$$\sigma_{\rm fus}(E_{\rm c.m.}) = \int_0^\infty D(B)\sigma_{\rm fus}^{(1)}(E_{\rm c.m.}, B)\,{\rm d}B, \tag{1}$$

based on the barrier penetrating model. Here we take $\sigma_{\rm fus}^{(1)}(E_{\rm c.m.}, B)$ to be Wong's formula [1] for the fusion cross section, which reads

$$\sigma_{\rm fus}^{(1)}(E_{\rm c.m.}, B) = \frac{\hbar\omega R_{\rm fus}^2}{2E_{\rm c.m.}} \ln\left(1 + \exp\left[\frac{2\pi}{\hbar\omega}(E_{\rm c.m.} - B)\right]\right), \tag{2}$$

where $E_{\rm c.m.}$ denotes the center-of-mass energy, and B, $R_{\rm fus}$ and $\hbar\omega$ are the height, the radius and the curvature of the barrier, respectively. $D(B)$ is a weight function to describe the distribution of the barrier heights and satisfies the normalization condition

$$\int_0^\infty D(B)\,{\rm d}B = 1. \tag{3}$$

Here, we assume that $D(B)$ consists of a set of Gaussian functions $G_i(B)$,

$$D(B) = \sum_{i=1}^{N} w_i G_i(B), \tag{4}$$

with

$$G_i(B) = \frac{1}{\sqrt{2\pi}L_i} \exp\left[-\frac{(B - B_i)^2}{2L_i^2}\right]. \tag{5}$$

Where, w_i, B_i and L_i are the weight, centroid and width of the ith Gaussian function, respectively. N is the number of Gaussian functions involved. By using expressions (1)–(5) the fusion excitation function can be calculated with the $3N + 1$ parameters in total, including the fusion radius $R_{\rm fus}$ and the curvature $\hbar\omega$ in equation (2) to be determined. By varying these parameters in a reasonable range, one can minimize the average deviation of fusion cross sections from the experimental data, defined as

$$\chi^2_{\rm log} = \frac{1}{m}\sum_{n=1}^{m}[\log(\sigma_{\rm th}(E_n)) - \log(\sigma_{\rm exp}(E_n))]^2 \tag{6}$$

with logarithmic scale for considering all of the measured fusion cross sections at energies from sub-barrier to over-barrier fusion. Here, m denotes the number of energy points of experimental data, $\sigma_{\rm th}(E_n)$ is calculated with equation (1) and $\sigma_{\rm exp}(E_n)$ is the experimental fusion cross section at the center-of-mass energy E_n. Then the optimal parameters (w_i, B_i, L_i) by which the distribution of barrier heights $D(B)$ is determined are obtained at the minimum of $\chi^2_{\rm log}$.

In principle, with an increasing number of Gaussian functions N, the distribution of barrier heights becomes more precise. However, the value of N is restricted by the computational cost and the number m of available energy points of experimental data. Therefore, one should make a compromise for a systematic study of the fusion barrier distributions. In this work, we take $N \leqslant 4$, the influence of the value of N on the distribution is discussed in the following part. In order to eliminate the influence of the fluctuation in experimental data caused by the statistical error, we randomly choose a part of experimental data when extracting the fusion barrier distribution at each time, by repeating such a procedure for many times we obtain the average barrier distribution with the weight being taken into account for each time.

The details of the procedure are as follows: first, we check the behavior of the measured fusion excitation function at over-barrier energies. As it is well known that the product $E\sigma_{\rm fus}$ at energies above the barrier increases linearly with energy according to the classical formula for fusion cross sections [5, 12]. Therefore, at over-barrier energies we can eliminate the data points which largely deviate from the linear dependence of $E\sigma_{\rm fus}$ versus E in extracting the barrier distribution from the measured fusion excitation function. Eliminating those data points at over-barrier energies will not make large effect on the barrier distribution. Then, at each time (we call each event, for convenience) for each data point we assign a random number ξ which is in a range of 0–1. If the random number ξ for a data point is larger than or equal to $P_{\rm accept}$, the data point will be chosen to be one of the data points for determining the barrier distribution in this event. Thus, only a part of the experimental data from the fusion excitation function is applied for extracting the barrier distribution in an event, while the $P_{\rm accept}$ will control the portion of the whole data points of the excitation function. Here $P_{\rm accept} = 0.2$ is taken. By performing such a procedure for $N_{\rm tot}$ times (i.e. producing $N_{\rm tot}$ events), we can obtain the average distribution of the fusion barrier heights $D_{\rm fus}(B)$, i.e.

$$D_{\rm fus}(B) = \frac{1}{C}\sum_{k=1}^{N_{\rm tot}} g_k D_k(B). \tag{7}$$

Where $D_k(B)$ and g_k are the obtained barrier distribution function and the relative weight of the kth event, respectively. The latter is estimated by

$$g_k = \frac{m_k}{m}\frac{\chi^2_{\rm log,max} - \chi^2_{{\rm log},k}}{\chi^2_{\rm log,max} - \chi^2_{\rm log,min}}, \tag{8}$$

the m_k and $\chi^2_{{\rm log},k}$ are the number of selected experimental data points and the corresponding deviation of the calculated fusion cross sections from the experimental data (see equation (6)) in the kth event, respectively. The $\chi^2_{\rm log,max}$ and $\chi^2_{\rm log,min}$ are the maximum and minimum deviation in the $N_{\rm tot}$ events, respectively. By using the relative weight g_k, the weight of each experimental data point is taken into account approximately. C in equation (7) is a normalization constant, i.e. $C = \sum_{k=1}^{N_{\rm tot}} g_k$. In this work, we set $N_{\rm tot} = 50$.

Figure 1 shows the fusion barrier distributions of ^{40}Ca+^{96}Zr [5] and ^{16}O+^{208}Pb [16] determined by the present method (solid curve) and by the double differentiation method (squares), i.e.

$$D_{\rm der}(E) = \frac{1}{\pi R^2_{\rm fus}}{\rm d}^2(E\sigma_{\rm fus})/{\rm d}E^2, \tag{9}$$

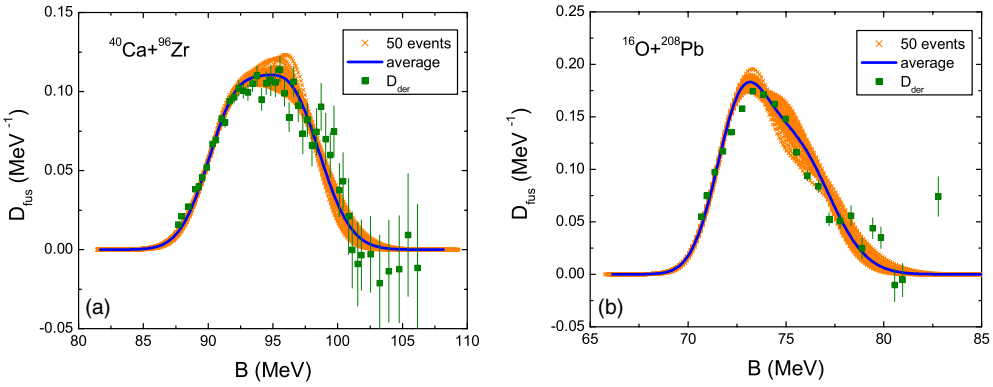

Figure 1. (Colour online) Distribution of the barrier heights of (a) ^{40}Ca+^{96}Zr and (b) ^{16}O+^{208}Pb. The solid curves and the squares denote the results of this approach $D_{\rm fus}(B)$ with $N = 2$ and those by equation (9), respectively. The crosses denote the results of 50 events. The fusion barrier distributions $D_{\rm der}$ are evaluated with the point-difference method in [4] by taking $\Delta E = 2.5$ MeV for all reactions in this work, if not otherwise stated.

respectively. The double differentiation is performed using the point difference method [4]. Here we take the number of Gaussian functions $N = 2$ in the calculations. It is seen from figure 1 that the barrier distributions determined by both methods are in good agreement. In order to show the fluctuation in the determined barrier distributions in a total of 50 events in the figure we also show the results of the 50 individual events by crosses, from which one can find the deviation of the barrier distribution in individual events from the average one. Obviously, the deviation is very small at the left side of the distribution while it is relatively large near the centroid and the right side of the distribution. It seems to be in accordance with the fact that the statistical error of $D_{\rm der}$ is proportional to the barrier energy. Figure 2 shows the distributions of barrier heights for the fusion reactions ^{28}Si+^{92}Zr [17], ^{32,34}S+^{89}Y [18], ^{36}S+^{110}Pd [19], ^{40}Ca+^{124}Sn [20], ^{48}Ca+^{154}Sm [21], ^{19}F+^{208}Pb [22] and ^{12}C+^{237}Np [23] determined by the two methods. Similarly, from figure 2 one sees that the fusion barrier distributions determined by both methods are in good agreement. In figure 2(c), we also show the results of the exact coupled channels calculations [18] including single-phonon states in ^{34}S and single-phonon (short dashed curve) and double-phonon states (dot-dashed curve) in ^{89}Y for comparison. The small peak in $D_{\rm fus}$ at energy about 79 MeV is well described by the coupled channels calculations with the excitations of the reaction partners being taken into account. In figure 2(h) we notice that a clearer picture of the shape of the barrier distribution is provided by using our method than the double differentiation method when the precision of the measured fusion excitation function is little lower. From the fluctuation of the distributions for the various events, the statistical errors of this approach are obtained and shown in shades in the sub-figures. With the statistical errors of the distributions, the standard deviations ΔB of the mean barrier heights and the deviations $\chi^2_{\rm log}$ of the cross sections which are also presented in the sub-figures, one may get a feeling for the reliability of the method and the precision of the obtained fusion barriers. To study the influence of the number of Gaussian functions involved, in figure 3 we show the distributions of barrier heights for ^{16}O+^{208}Pb determined by setting the number of Gaussian functions from $N = 1$ to $N = 4$, respectively. The squares denote the $D_{\rm der}$ for comparison. The inserted figure in figure 3 presents the deviations of the fusion excitation functions from the measured experimental data for the four cases with $N = 1$–4, respectively. One finds that when $N = 1$, the deviation of the calculated

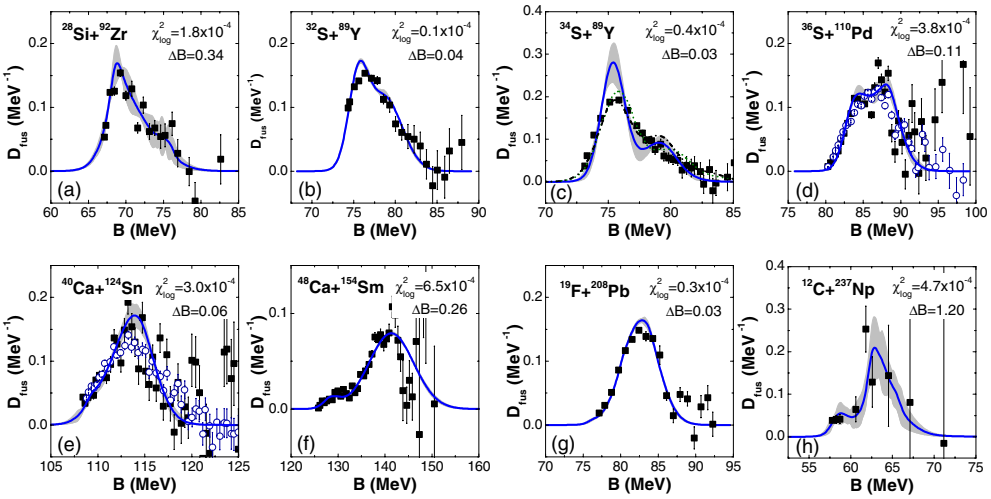

Figure 2. (Colour online) Distribution of the barrier heights of reactions ^{28}Si+^{92}Zr, ^{32,34}S+^{89}Y, ^{36}S+^{110}Pd, ^{40}Ca+^{124}Sn, ^{48}Ca+^{154}Sm, ^{19}F+^{208}Pb and ^{12}C+^{237}Np. The solid curves and the squares denote the results of this approach $D_{\rm fus}(B)$ with $N = 2$ and those obtained with equation (9) by taking $\Delta E = 2.5$ MeV, respectively. The open circles in (d) and (e) denote the results obtained with equation (9) by taking $\Delta E = 4.0$ MeV. The shades denote the statistical errors due to the fluctuations of the Gaussian fits for 50 events, and the average deviations $\chi^2_{\rm log}$ of the cross sections and the standard deviations ΔB (in MeV) of the mean barrier heights are also presented in the sub-figures. The dot-dashed curve in (c) is a coupled channel calculation from [18].

fusion excitation function from the experimental data is about 5×10^{-4} and for this case, the centroid of the barrier distribution is roughly reproduced whereas the right side part of the distribution is not reproduced well. For $N = 2$, the deviation decreases sharply, down to less than 0.3×10^{-4}. When the number of Gaussian functions further increases, we find the deviation of the fusion excitation function from the measured data decreases slowly. The obtained barrier distributions with $N = 4$ and $N = 3$ are very close to each other. Here we should state that the number of Gaussian functions to fit the barrier distribution is not identical with the number of barriers involved, it is only a feature of the fit procedure.

In table 1, we list the obtained mean barrier heights of some selected reactions using the proposed method with the number of Gaussian functions $N = 1$, 2 and 3, respectively. The fusion barriers given in [12] and [8] which are mentioned in the previous section are also listed for comparison. In addition, we also list the mean barrier heights $B_{\rm th}$ of the empirical barrier distributions proposed in [14] which will be discussed in the following section. One finds that the fusion barriers of [8] which were obtained by fitting the experimental data at energies above the average barriers are systematically higher than the corresponding barriers of [12] which were obtained by using the single Gaussian fitting procedure. In this work, the obtained mean barrier heights $B_{\rm m}$ are very close to those of [12] when taking $N = 1$. We find that the most probable fusion barriers of the reactions are reproduced well with the single Gaussian fitting procedure. When taking $N = 2$, the obtained $B_{\rm m}$ increase for most of the reactions listed in the table, which indicates that the fusion barrier distribution is not symmetric generally and the right side (high energy part) of the distribution is broader than the left side for most of the selected reactions. The asymmetric character of the distribution has been found by both experiments and theoretical analysis and been taken into account in empirical barrier distribution functions (see [14, 27]). The differences between the obtained mean barrier

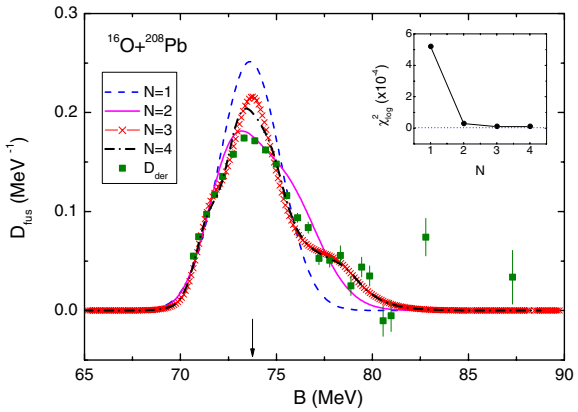

Figure 3. (Colour online) Distribution of the barrier heights of ^{16}O+^{208}Pb. The dashed, solid, crossed and dash-dotted curves denote the $D_{\rm fus}(B)$ with the number of Gaussian functions from $N = 1$ to $N = 4$, respectively. The squares denote the results obtained with equation (9). In the inserted figure, the average deviations from the measured fusion cross sections are shown as a function of N.

Table 1. Fusion barriers obtained with different methods.

Reaction	Data in [12]	$B_{\rm m}$ ($N = 1$)	$B_{\rm m}$ ($N = 2$)	$B_{\rm m}$ ($N = 3$)	Data in [8]	$B_{\rm th}$
^{16}O+^{144}Sm [4]	60.5	60.23	60.95	60.91	61.03	60.86
^{17}O+^{144}Sm [4]	60.6	60.24	60.25	60.34	60.57	60.52
^{16}O+^{148}Sm [4]	59.4	59.64	59.71	59.71	59.83	60.46
^{16}O+^{154}Sm [4]	58.4	58.63	59.18	59.22	59.35	59.73
^{16}O+^{186}W [4]	68.3	67.92	68.62	68.63	68.87	69.13
^{16}O+^{208}Pb [16]	73.6	73.63	74.18	74.35	74.52	75.06
^{19}F+^{208}Pb [22]	–	82.59	82.52	82.50	82.96	83.65
^{16}O+^{92}Zr [17]	–	41.41	41.43	41.49	41.96	41.98
^{28}Si+^{92}Zr [17]	–	70.01	70.65	70.65	70.93	70.98
^{36}S+^{90}Zr [24]	77.0	77.02	77.66	77.48	77.97	79.55
^{36}S+^{96}Zr [24]	74.9	74.77	75.73	75.44	75.61	78.54
^{40}Ca+^{46}Ti [25]	57.3	57.28	57.78	57.52	57.89	59.20
^{40}Ca+^{48}Ti [25]	57.1	57.12	57.43	57.35	57.88	58.71
^{40}Ca+^{50}Ti [25]	57.3	56.92	57.23	57.23	58.21	58.21
^{40}Ca+^{90}Zr [5]	96.1	96.09	96.37	96.30	96.88	99.24
^{40}Ca+^{96}Zr [5]	93.6	93.64	94.46	94.41	94.59	97.80
^{40}Ca+^{48}Ca [26]	51.8	51.66	51.51	51.59	52.00	52.81
^{48}Ca+^{48}Ca [26]	51.2	51.13	51.41	51.32	51.49	51.47

heights with $N = 2$ and with $N = 3$ are very small and the deviations are smaller than 0.5%. Table 1 and figure 3 indicate that one can get a reasonable balance between accuracy and computational cost if taking two Gaussian functions for approximately describing the fusion barrier distributions.

In table 2, we list the corresponding fusion radii $R_{\rm fus}$ of the reactions in table 1 with the proposed method and the methods in [8, 12]. We find that the extracted fusion radii based on the same fusion excitation functions are different with different methods. The differences of

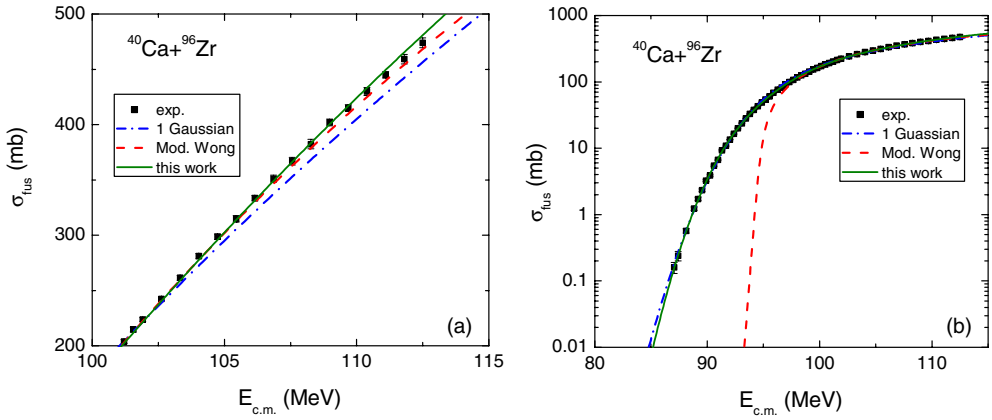

Figure 4. (Colour online) Fusion excitation function of ^{40}Ca+^{96}Zr. The dash-dotted and the dashed curves denote the calculated results with the methods in [8, 12], respectively. The solid curves denote the results with the proposed method by taking $N = 2$. The squares denote the experimental data.

Table 2. Fusion radii obtained with different methods.

Reaction	Data in [12]	R_{fus} ($N = 1$)	R_{fus} ($N = 2$)	R_{fus} ($N = 3$)	Data in [8]
^{16}O+^{144}Sm [4]	10.3	10.06	10.63	10.61	10.85
^{17}O+^{144}Sm [4]	10.8	10.43	10.44	10.49	10.79
^{16}O+^{148}Sm [4]	10.2	10.44	10.52	10.51	10.76
^{16}O+^{154}Sm [4]	9.6	9.91	10.45	10.48	10.76
^{16}O+^{186}W [4]	10.6	10.24	10.78	10.78	11.12
^{16}O+^{208}Pb [16]	10.5	10.46	10.92	11.02	11.31
^{19}F+^{208}Pb [22]	–	11.06	11.04	11.03	11.50
^{16}O+^{92}Zr [17]	–	9.52	9.54	9.55	10.02
^{28}Si+^{92}Zr [17]	–	9.49	9.87	9.88	10.19
^{36}S+^{90}Zr [24]	10.8	10.83	11.47	11.30	10.54
^{36}S+^{96}Zr [24]	11.0	10.84	11.73	11.51	10.79
^{40}Ca+^{46}Ti [25]	9.4	9.60	10.00	9.81	9.77
^{40}Ca+^{48}Ti [25]	9.4	9.65	9.79	9.76	9.85
^{40}Ca+^{50}Ti [25]	9.4	9.26	9.51	9.52	9.84
^{40}Ca+^{90}Zr [5]	10.0	9.92	10.13	10.09	10.53
^{40}Ca+^{96}Zr [5]	9.3	9.27	9.82	9.80	10.12
^{40}Ca+^{48}Ca [26]	11.5	11.29	11.17	11.22	9.99
^{48}Ca+^{48}Ca [26]	11.2	11.06	11.43	11.33	10.16

the fusion radii obtained in [12] and those in [8] are quite large for some reactions, for example, the differences are larger than 1 fm for the reactions ^{40,48}Ca+^{48}Ca and ^{16}O+^{154}Sm. With the proposed method, the fusion radii can also be obtained. The obtained results with $N = 3$ and those with $N = 2$ are close to each other and the differences between them $\Delta R_{fus} \leqslant 0.1$ fm for most of the selected reactions. In order to understand the differences of the results due to the different methods, we studied the fusion cross sections of ^{40}Ca+^{96}Zr. Figure 4 shows the calculated fusion excitation functions in [8, 12] and that with the proposed method by taking $N = 2$. In order to see the results more clearly, in figures 4(a) and (b) we adopt linear and logarithmic scale for the fusion cross sections, respectively. One finds that the fusion cross sections are reproduced better with the modified Wong formula adopted in [8] than that with

Table 3. Obtained fusion barrier distributions for some selected reactions using the proposed method with the number of Gaussians $N = 2$.

Reaction	FWHM (MeV)	a_L (MeV)	B_m (MeV)	R_{fus} (fm)	$\chi^2_{log} \times 10^{-4}$
^{16}O+^{144}Sm [4]	1.61	1.43	60.95	10.63	5.7
^{17}O+^{144}Sm [4]	3.45	2.80	60.25	10.44	3.5
^{16}O+^{148}Sm [4]	4.38	4.36	59.71	10.52	2.1
^{16}O+^{154}Sm [4]	4.50	5.66	59.18	10.45	13.4
^{16}O+^{208}Pb [16]	5.46	2.38	74.18	10.92	0.3
^{19}F+^{208}Pb [22]	5.52	4.19	82.52	11.04	0.3
^{40}Ca+^{90}Zr [5]	3.63	2.08	96.37	10.13	1.3
^{40}Ca+^{96}Zr [5]	8.78	4.59	94.46	9.82	0.6
^{40}Ca+^{48}Ca [26]	3.36	2.45	51.51	11.17	7.0
^{48}Ca+^{48}Ca [26]	3.15	1.33	51.41	11.43	3.3

the single Gaussian fitting procedure proposed in [12] at energies above the average fusion barriers, but the latter gives much better results at sub-barrier fusion. It means that the former method focuses on the above-barrier fusion while the latter one seems to be more suitable for describing fusion reaction at energies near the average barrier. With our proposed method, the fusion cross sections at energies both below and above the average barrier can be reproduced remarkably well (with $\chi^2_{log} = 0.6 \times 10^{-4}$).

Now let us discuss the characteristics of the fusion barrier distributions. With the barrier distribution determined with $N = 2$, the mean barrier height, the width and especially the diffuseness of both sides of the distribution can be obtained. In table 3, we list the full widths at half maximum (FWHM) of the distributions and the left diffuseness a_L of the distributions for some selected reactions. The a_L is defined as the barrier height difference between the 10% of maximum and 90% of maximum at the left side of the distribution. We also list in the table the mean barrier heights B_m, the corresponding fusion radii R_{fus} of the determined barrier distributions of those reactions and the corresponding average deviation χ^2_{log}. From table 3 one sees that the values of left diffuseness a_L increase obviously from ^{16}O+^{144}Sm, ^{16}O+^{148}Sm to ^{16}O+^{154}Sm which shows the same tendency as the sub-barrier fusion cross sections of those reactions (see [14]). One can also find that the a_L values for ^{40}Ca+^{90}Zr and ^{48}Ca+^{48}Ca are much smaller than those of ^{40}Ca+^{96}Zr and ^{40}Ca+^{48}Ca, which is consistent with the fact that the sub-barrier fusion cross sections for ^{40}Ca+^{90}Zr and ^{48}Ca+^{48}Ca are much smaller than those of ^{40}Ca+^{96}Zr and ^{40}Ca+^{48}Ca. Thus, it seems to us that the left diffuseness of the fusion barrier distribution is closely related to the enhancement and suppression effect of sub-barrier fusion cross sections due to structure effects.

3. Theoretical description of the fusion barriers

In this section, we first present a systematic comparison between the characteristics of the fusion barrier distributions determined by the proposed method and those of empirical distributions based on the nucleus–nucleus potentials calculated with the Skyrme energy-density functional within the extended Thomas–Fermi approach for 120 fusion reactions. Then, the influence of the static deformation and the deformation due to excitation of the reaction partners on the reduction of the fusion barriers will be studied for a series of reactions induced by ^{16}O. Finally, some different nuclear potentials will be investigated by comparing the corresponding calculation results.

3.1. Empirical barrier distribution

In our previous paper [14], we applied the Skyrme energy-density functional to study heavy-ion fusion reactions. The barriers for fusion reactions were calculated by the Skyrme energy-density functional together with the semi-classical extended Thomas–Fermi method [28]. Based on the potential barrier obtained, we proposed a parametrization of the empirical barrier distribution which is a superposition of two Gaussian functions to take into account the multi-dimensional character of the real barrier and then applied it to calculate the fusion excitation functions of light and intermediate–heavy fusion systems in terms of the barrier penetration concept. A large number of measured fusion excitation functions at energies around the fusion barriers were reproduced well. Now we make a systematic comparison of the parametrization of the empirical barrier distributions with those determined by the method given in this work.

For the reader's convenience, the empirical barrier distribution is briefly introduced here. We assume the weight function $D(B)$ in equation (1) to be a superposition of two Gaussian functions $D_1(B)$ and $D_2(B)$,

$$D_1(B) = \frac{\sqrt{\gamma}}{2\sqrt{\pi}b_1}\exp\left[-\gamma\frac{(B-B_1)^2}{(2b_1)^2}\right] \tag{10}$$

and

$$D_2(B) = \frac{1}{2\sqrt{\pi}b_2}\exp\left[-\frac{(B-B_2)^2}{(2b_2)^2}\right], \tag{11}$$

with

$$b_1 = \tfrac{1}{4}(B_0 - B_c), \tag{12}$$

$$b_2 = \tfrac{1}{2}(B_0 - B_c), \tag{13}$$

$$B_1 = B_c + b_1, \tag{14}$$

$$B_2 = B_c + b_2. \tag{15}$$

Here B_0 is the height of the potential barrier obtained with the Skyrme energy-density functional together with the semi-classical extended Thomas–Fermi method [14]. The quantity $B_c = fB_0$ is the effective barrier height empirically taking into account the coupling effects to other degrees of freedom, such as dynamic deformation. We set the reduction factor $f = 0.926$ for the Skyrme interaction SkM* [29], which is the same as in [14]. Based on $D_1(B)$ and $D_2(B)$, an effective weight function $D_{\rm eff}(B)$ by which the fusion excitation function can be calculated, is proposed,

$$D_{\rm eff}(B) = \begin{cases} D_1(B) & : \quad B < B_x \\ D_{\rm avr}(B) & : \quad B \geqslant B_x, \end{cases} \tag{16}$$

with $D_{\rm avr}(B) = (D_1(B) + D_2(B))/2$. The B_x denotes the position of the left crossing point between $D_1(B)$ and $D_{\rm avr}(B)$. According to equations (10)–(16) the peak and the width of $D_{\rm eff}(B)$ only depend on the height of the potential barrier B_0 except the γ in $D_1(B)$. The quantity γ in $D_1(B)$ is a factor which empirically takes into account the structure effects [14]. For the fusion reactions with non-closed-shell nuclei but near the β-stability line and for the fusion reactions at energies near and above the barrier we set $\gamma = 1$. With the effective weight function $D_{\rm eff}(B)$, the mean barrier height $B_{\rm th} = \int B D_{\rm eff}(B)\,{\rm d}B \big/ \int D_{\rm eff}(B)\,{\rm d}B$, the

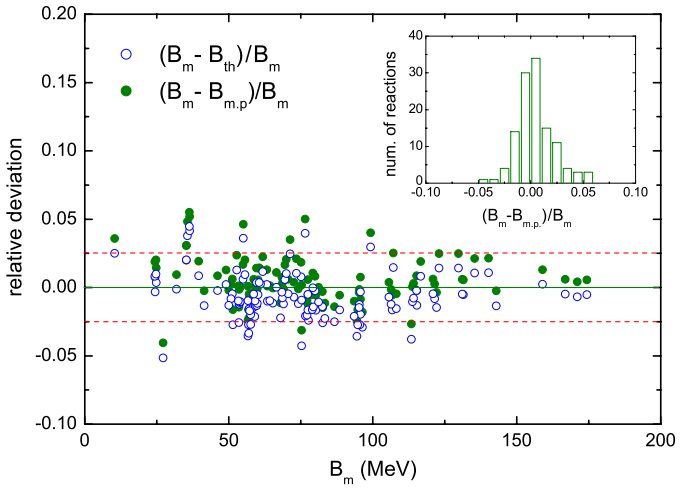

Figure 5. (Colour online) Relative deviations of the extracted mean barrier height $B_{\rm m}$ from the calculated mean barrier height $B_{\rm th}$ (open circles) and the most probable barrier height $B_{\rm m.p.}$ (solid circles) for 120 fusion reactions. The distribution of the deviations between $B_{\rm m}$ and $B_{\rm m.p.}$ for these reactions is shown in the inserted figure.

most probable barrier height $B_{\rm m.p.}$ and the FWHM of the distribution can be easily obtained. $B_{\rm th}$ is always slightly higher than $B_{\rm m.p.}$ because of the shape of $D_{\rm eff}(B)$. The calculated mean barrier heights by setting $\gamma = 1$ for some reactions are listed in table 1.

We have investigated the fusion barrier distributions for a total of 120 fusion reactions from light to intermediate–heavy systems. In figure 5, we show the relative deviations of the extracted mean barrier height $B_{\rm m}$ from $B_{\rm th}$ and $B_{\rm m.p.}$ by taking $N = 2$ and calculated with $D_{\rm eff}(B)$ by setting $\gamma = 1$, respectively. From the figure, one sees that the relative deviations between $B_{\rm m}$ and $B_{\rm th}$ are smaller than 0.025 for more than 80% reactions. In addition the most probable barrier heights $B_{\rm m.p.}$ are also close to the extracted $B_{\rm m}$ and the relative deviations between $B_{\rm m}$ and $B_{\rm m.p.}$ (solid circles) are smaller than 0.025 for 88% reactions and 0.01 for 54% reactions. In figure 6 we compare the fusion radii $R_{\rm fus}$ extracted by the proposed method with those of the entrance-channel fusion potentials obtained with the Skyrme energy-density functional together with the extended Thomas–Fermi approach [14] for the 120 reactions. The extracted fusion radii are reproduced reasonably well. Figures 5 and 6 indicate that the global features of the empirical barrier distributions proposed in [14] are in good agreement with those of the barrier distributions determined by the present method.

In figure 7 we present a comparison between the extracted fusion barrier distributions $D_{\rm der}$ and the empirical ones $D_{\rm eff}$ for the reactions ^{12}C+^{92}Zr, ^{19}F+^{208}Pb and ^{16}O+^{144,154}Sm. The squares and the crossed curves denote the results for $D_{\rm der}$ and $D_{\rm eff}$, respectively. The shapes of the fusion barrier distributions extracted from experimental data are well reproduced by the parametrization of the empirical barrier distribution proposed in [14].

By using the proposed empirical barrier distribution, the fusion barriers of a large number of reactions can be described reasonably well, which indicates that (1) the model is very useful for prediction of the fusion barriers and the fusion cross sections of unmeasured fusion systems; (2) there exist some similar characteristics of the fusion barriers in the reactions with either deformed nuclei or spherical nuclei. For understanding the physics behind the fusion barrier distributions, the influence of the deformation of the reaction partners on the reduction of the fusion barriers is investigated in the following subsection.

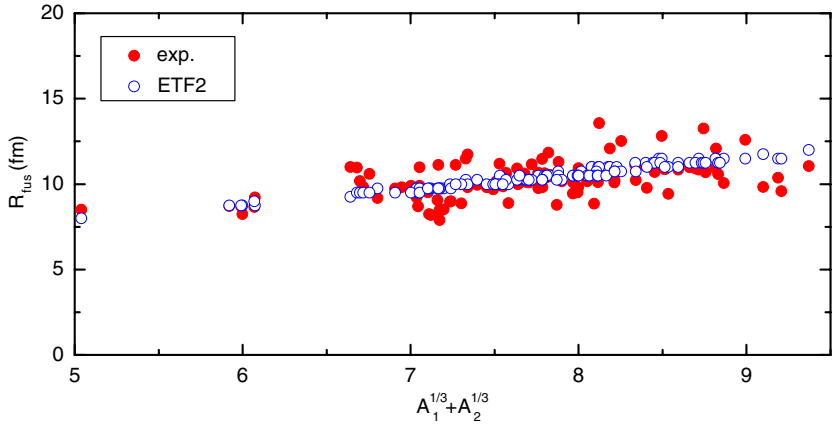

Figure 6. (Colour online) Fusion radii of 120 selected reaction systems. The solid and open circles denote the extracted results with $N = 2$ and the calculated results with the Skyrme energy-density functional together with the extended Thomas–Fermi approach (ETF2), respectively. A_1 and A_2 denote the mass numbers of the projectile and target nuclei, respectively.

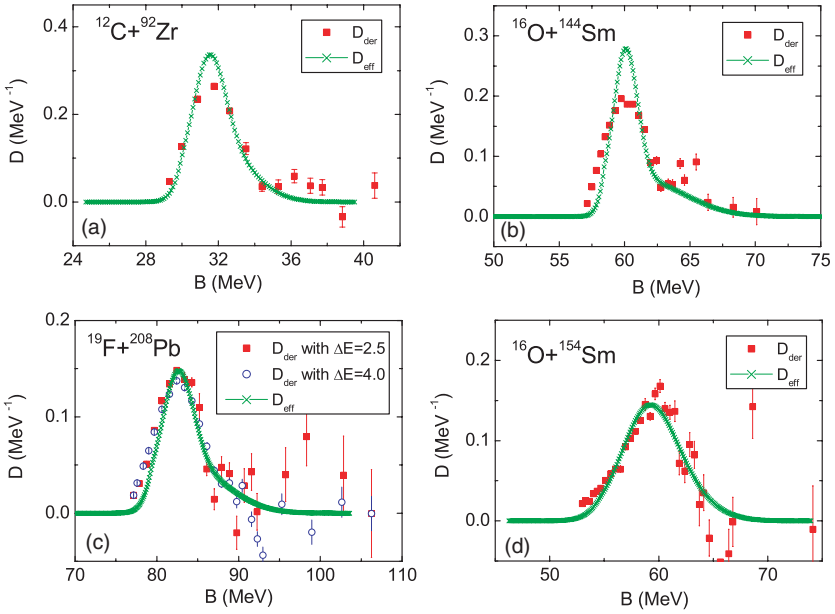

Figure 7. (Colour online) Fusion barrier distributions for the reactions $^{12}C+^{92}Zr$, $^{19}F+^{208}Pb$ and $^{16}O+^{144,154}Sm$. The squares and the crossed curves denote the results for D_{der} and D_{eff}, respectively.

3.2. Reduction of fusion barrier due to deformation of nuclei

We should mention that the entrance-channel potential obtained with the Skyrme energy-density approach is based on the frozen-density approximation; therefore it gives the uncoupled fusion potential of a reaction system which could be higher than the average fusion barrier energy of the system extracted experimentally. In this work, the influence of the deformation

of nuclei on the reduction of the fusion barriers is systematically explored for a series of fusion reactions with ^{16}O projectile nuclei. The entrance-channel potential for a certain reaction is calculated with the Skyrme energy-density functional together with the ETF2 approach in which the deformation and orientation of the target nuclei are taken into account. The density distributions of protons ($i = p$) and neutrons ($i = n$) of the reaction partners are taken to be deformed Fermi distribution for convenience, which reads

$$\rho_i(\mathbf{r}, \theta) = \rho_{0i}\left[1 + \exp\left(\frac{r - R(\theta)}{a_i}\right)\right]^{-1}, \qquad i = \{n, p\}, \tag{17}$$

with

$$R(\theta) = R_{0i}\left(1 + \sum_{\lambda \geqslant 2} \beta_\lambda Y_{\lambda 0}(\theta)\right) \tag{18}$$

for an axially symmetric deformed or deformable nucleus. Here $\vec{\beta} \equiv \{\beta_\lambda\}$ are dimensionless deformation parameters of multi-polarity $\lambda = 2, 3, 4, 5\ldots$ and $Y_{\lambda 0}$ are the corresponding spherical harmonics. In this work, we assume that the surface diffuseness a_i and the radius R_{0i} of the nucleus are frozen and taken as the corresponding results of the spherical framework [14] for the sake of simplicity. The central densities ρ_{0i} are obtained according to the conservation of particle numbers. We have checked the central densities of heavy nuclei when the deformation parameters are varied and found that the change of ρ_{0i} with $\vec{\beta}$ is quite small. In addition we have checked the entrance channel fusion barriers with the densities determined by the Skyrme Hartree–Fock calculations and by the Fermi distributions within the restricted density variational approach for a series of reactions induced by ^{16}O, and found that the deviations of the barrier heights between the two cases are about 1–2 MeV (the barriers in the latter case are higher due to the smaller surface diffuseness of the obtained densities with ETF2 for the reaction partners [14]).

The influence of the static quadrupole deformation of deformed target nuclei on the fusion barriers is investigated for fusion reaction ^{16}O+^{154}Sm. We study the influence of the orientation angle Θ between the symmetry axis of the deformed target nuclei and the line connecting the centers of the nuclei on the entrance-channel potential for ^{16}O+^{154}Sm. For this reaction the lowest barrier is obtained for the orientation $\Theta = 0^\circ$, i.e. when ^{16}O touches the tip of the deformed ^{154}Sm target, while the highest barrier is obtained for $\Theta = 90^\circ$, when ^{16}O touches the side, as shown in figure 8. The lowest barrier is close to the extracted most probable fusion barrier denoted by the dashed arrow in figure 8. The fusion barrier B_0 obtained without the deformation of ^{154}Sm taken into account is also shown in figure 8 by the solid arrow for comparison. One sees that the fusion barrier B_0 is reduced by about 6% due to the static quadrupole deformation of the target. For fusion reactions ^{16}O+^{186}W and ^{16}O+^{238}U, we get the same conclusion. From figure 8 one can also learn that there exists a distribution of the barrier heights due to the variation of the orientation angle Θ of the deformed target. We then investigate the relations between the FWHMs of the fusion barrier distributions and the orientations of the deformed targets for the fusion reactions with ^{16}O and ^{48}Ca bombarding on the deformed targets ^{154}Sm, ^{186}W and ^{238}U. The differences between the barriers obtained with $\Theta = 90^\circ$ and those with $\Theta = 0^\circ$, denoted by $B^{(90)} - B^{(0)}$, are obtained and shown in figure 9. The extracted FWHMs of the barrier distributions determined by the proposed method are also shown for comparison. In addition, the FWHM of the empirical barrier distribution $D_{\text{eff}}(B)$ (see equations (10)–(16)) can be approximately expressed as a function of B_0 with $\gamma = 1$,

$$\text{FWHM} \approx 0.0755 B_0. \tag{19}$$

One sees that the extracted FWHMs of the barrier distributions are comparable with the largest barrier differences $B^{(90)} - B^{(0)}$ due to different orientations which can be well described with

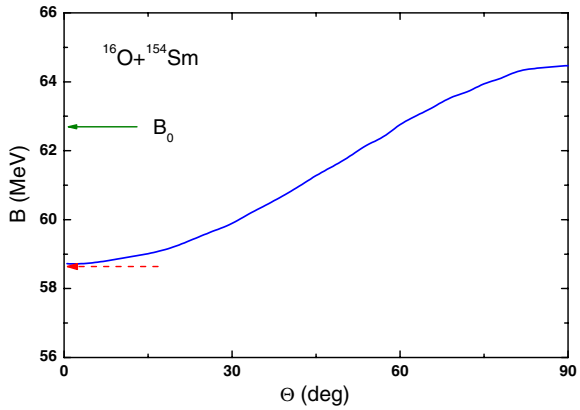

Figure 8. Height of the fusion barrier as a function of the orientation of the deformed target for ^{16}O+^{154}Sm. Here the static quadrupole deformation β_2 of ^{154}Sm is determined with the finite range droplet model (FRDM) [31]. The dashed arrow denotes the extracted most probable fusion barrier. The solid arrow gives the fusion barrier calculated without the deformation of the target taken into account.

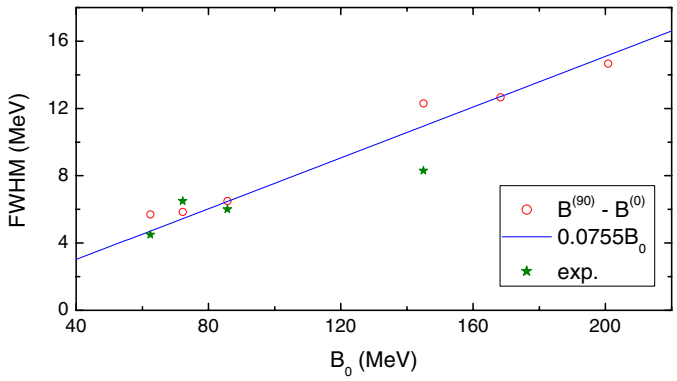

Figure 9. FWHMs of fusion barrier distributions for reactions with ^{16}O and ^{48}Ca bombarding on the deformed targets ^{154}Sm, ^{186}W and ^{238}U. The open circles denote the largest barrier differences $B^{(90)} - B^{(0)}$ due to different orientations, the solid line denotes the results with equation (19). The extracted FWHMs of the barrier distributions are also presented by the stars.

equation (19). It indicates that (1) the variation of the orientations of the deformed target plays a role for the width of the barrier distribution; (2) the influence of the static deformation of the reaction partners on the fusion barriers is partly taken into account in the empirical barrier distribution.

Similarly, for fusion reactions with near-spherical nuclei, the surface vibration of nuclei will also affect the barrier distribution. It was shown in [27] that dynamic deformation of nuclei plays an important role for the fusion barrier. In this work, we investigate the reduction of the fusion barriers due to the deformation of the reaction partners caused by excitation with the Skyrme energy-density functional together with the extended Thomas–Fermi approach. It is known that the total energy of the reaction system is uniquely determined by the density distributions of the system based on the Skyrme energy-density functional approach [14]. Therefore the potential energy surface $E_{\rm tot}(R, \vec{\beta}^{p}, \vec{\beta}^{t})$ of the reaction system can be obtained

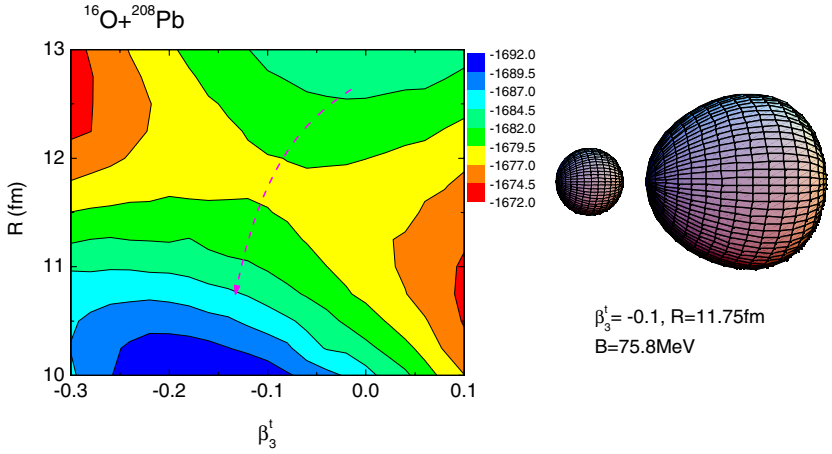

Figure 10. (Colour online) Potential energy surface of ^{16}O+^{208}Pb. The dashed line shows a possible dynamic fusion path. The corresponding shape of the reaction partners at the saddle point is drawn at the right side of the figure.

and expressed as a function of the distance R between two nuclei and the deformation of the projectile $\vec{\beta}^p$ and of the target $\vec{\beta}^t$ when the densities are determined by equation (18) and the orientation angle is set as zero. According to the potential energy surface, one may obtain the quasi-adiabatic fusion barrier. In order to distinguish the deformation of nuclei due to excitation from the static deformation of ground state nuclei, we call the deformation of near-spherical nuclei caused by excitation in fusion process non-ground-state deformation in this work. We first investigate the influence of non-ground-state octupole deformation β_3 of ^{208}Pb on the fusion barriers in reaction ^{16}O+^{208}Pb, since it is known that the 2.615 MeV 3^- vibration state of ^{208}Pb is the first excitation state which is usually taken into account in the fusion-coupled channel calculation [32]. Figure 10 shows the potential energy surface for this reaction when taking the distance R and the octupole deformation β_3^t of ^{208}Pb into account and setting the other deformation parameters to zero. One finds that there exists a saddle point at deformation $\beta_3^t = -0.1$ and distance $R = 11.75$ fm. The minus sign in the β_3^t of ^{208}Pb means that the target has a nose toward the projectile nucleus (see figure 10). It indicates that the non-ground-state octupole deformation of ^{208}Pb influences the fusion process, and a possible dynamic fusion path is shown in the figure by a dashed line. This static method only roughly gives the possible dynamical fusion path. More realistic dynamic process should be described with the time-dependent Hartree–Fock (TDHF) calculations [9–11]. Comparing with the uncoupled fusion barrier $B_0 = 78.5$ MeV, the fusion barrier is reduced by 2.7 MeV due to the octupole deformation of ^{208}Pb. When the β_5 of ^{208}Pb is simultaneously taken into account (the next excitation state of ^{208}Pb is the 3.198 MeV 5^- state), the fusion barrier is reduced to 74.2 MeV. And when the octupole deformation of ^{16}O is further involved, the fusion barrier is continuously lowered to 73.7 MeV which is very close to the extracted most probable fusion barrier and shown in figure 3 by the solid arrow.

The influence of the non-ground-state quadrupole and octupole deformations of the target on the fusion barriers is studied systematically for a series of fusion reactions with ^{16}O bombarding on near-spherical nuclei such as ^{16}O, ^{92}Zr, ^{112,116}Sn, ^{144}Sm and so on. For most even-even near-spherical nuclei the low-lying 2^+ vibration state is the first excitation state. We calculate the fusion barrier at the saddle point when β_2 is taken into account similar to

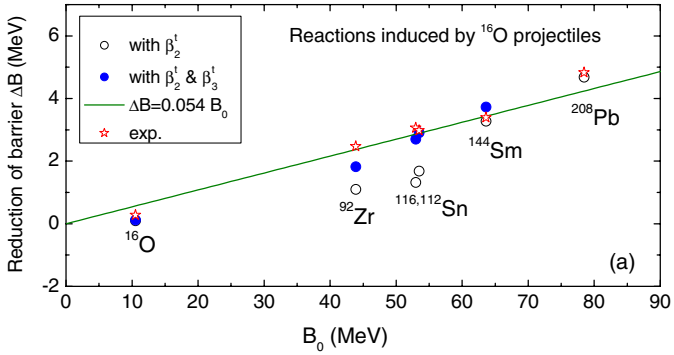

Figure 11. (Colour online) Reduction of fusion barriers due to non-ground-state quadrupole and octupole deformations of target nuclei. The open and solid circles denote the results with β_2 and with both β_2 and β_3 of target taken into account, respectively. The stars denote the difference of the barriers between the uncoupled fusion barrier B_0 and the extracted most probable fusion barrier. The solid line denotes the results obtained with the empirical barrier distributions (see equation (20)).

figure 10. Figure 11 shows the relation between the reduction of the fusion barrier ΔB and the uncoupled fusion barrier B_0 for these reactions. The open and solid circles denote the results with β_2 and with both β_2 and β_3 of the target nuclei taken into account, respectively. The stars denote the reduction of the fusion barriers based on the extracted most probable fusion barriers. In addition, based on the empirical barrier distribution mentioned in the above sub-section, the difference of the barriers between the uncoupled fusion barrier B_0 and the most probable barrier calculated with equations (10)–(16) by setting $\gamma = 1$ can be obtained and an approximated expression

$$\Delta B \approx 0.054 B_0 \tag{20}$$

is given with good accuracy. From the figure, one finds that the reductions of the fusion barriers increase with the barrier heights. The calculated reductions of the barriers due to the non-ground-state deformations of the target nuclei are close to the experimental data which can be described reasonably well with equation (20). It seems to us that the fusion barriers are systematically reduced by about 5% due to the non-ground-state deformation of the near-spherical nuclei. In [32] the authors studied the fusion reaction ^{16}O+^{208}Pb by using the fusion-coupled channel model and found that the inclusion of couplings to the target and projectile excitation states effectively reduces the uncoupled barrier height by 3.8 MeV (5%) in total, which is consistent with our estimation.

Figure 12 shows the relation between the obtained non-ground-state quadrupole deformation β_2^t and the mass $A_{\rm targ}$ of the target nuclei for a series of reactions induced by ^{16}O. One finds that the obtained non-ground-state quadrupole deformations increase with the size of the target nuclei generally. For heavy targets, the obtained β_2^t is about 0.24 which is comparable with the static quadrupole deformations of the lanthanides and actinides. From the above discussion about the barrier reduction due to the static deformation of nuclei, we learn that the lowest barrier of the reaction system is obtained when ^{16}O touches the tip of the prolate deformed target, and is close to the most probable fusion barrier. This indicates that the reduction of the fusion barriers due to the static deformation in fusion reactions with deformed nuclei and that due to the deformation caused by excitation in reactions with near-spherical nuclei are comparable, and the corresponding barrier reduction factors are close to each other.

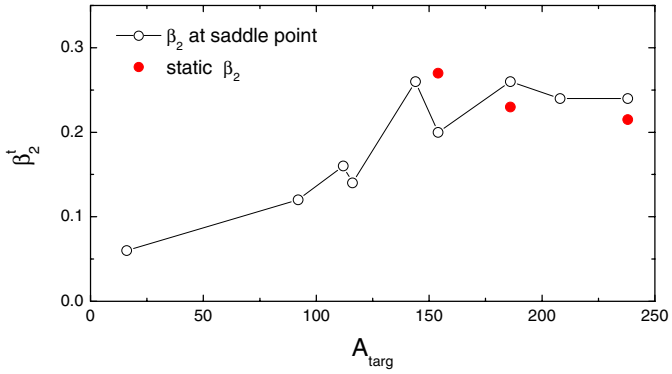

Figure 12. Relation between the obtained non-ground-state quadrupole deformation (open circles) and the mass number of the target nuclei for a series of reactions induced by ^{16}O. The deformation of the targets are obtained at the saddle points of the potential energy surface $E_{\rm tot}(R, \vec{\beta}^p, \vec{\beta}^t)$. The solid circles denote the static quadrupole deformations of ^{154}Sm, ^{186}W and ^{238}U obtained with the FRDM model [31].

3.3. Comparisons among different nuclear interactions

Finally, let us discuss the reduction factor of the empirical barrier distribution which appeared in equations (10)–(16). In the parametrization of the empirical barrier distribution proposed in [14], a reduction factor f for the effective barrier is introduced to take into account the coupling effect to other degrees of freedom, which in principle should depend on the effective interaction adopted. Now we study how the reduction factor f changes when a different effective interaction is adopted. As proposed in [14] except the factor γ which is introduced for considering the structure effect of the reaction partners, the parametrization of the barrier distribution for a fusion reaction is completely determined by the potential barrier B_0 which is calculated with the Skyrme energy-density functional together with the extended Thomas–Fermi approach including all terms up to second order in the spatial derivatives (ETF2). Then combining the parametrization of the barrier distribution with Wong's formula, the fusion excitation function can be calculated with equation (1). The f as a fitting parameter can be obtained by minimizing the average deviation $\chi^2_{\rm log}$ of the calculated fusion excitation function with B_0 from the corresponding experimental data. In this work, the experimental data of the fusion excitation functions at energies above the potential barriers for 120 fusion reactions from light to intermediate–heavy systems are used to search for the optimal value of the reduction factor for different Skyrme forces. In addition, for the widely used proximity potential [33] and Woods-Saxon potential [7], the reduction factors are also investigated. Table 4 lists the obtained optimal reduction factor $f_{\rm opt}$ and the minimal average deviation $\chi^2_{\rm log,m}$. One can see from table 4 that the $\chi^2_{\rm log,m}$ values for the Skyrme energy-density functional together with the ETF2 approach are smaller than those found with both the macroscopic Woods-Saxon and proximity potential. The minimal average deviation $\chi^2_{\rm log,m}$ by the proximity potential (Prox.) is obviously smaller than that by the Woods-Saxon potential (W-S.), which indicates that the former describes the fusion excitation function systematically better than the latter. The $\chi^2_{\rm log,m}$ for the case using the SIII interaction, which has a very large compressibility modulus $K_\infty = 355$ MeV, is the largest one among those obtained with Skyrme interactions, while the $\chi^2_{\rm log,m}$ for the case using the SkM* interaction is the smallest. In addition, the optimal value $f_{\rm opt}$ of the reduction factor obtained by this method for the SkM* force is 0.927, which is very close to that we adopted in [14].

Table 4. Optimal value $f_{\rm opt}$ of the reduction factor and the corresponding minimal deviation $\chi^2_{\rm log,m}$ from the experimental data of fusion excitation functions for 120 fusion reactions.

interaction	W-S. [7]	Prox. [33]	SIII [34]	SkP [35]	SLy4 [36]	SLy7 [36]	BSk8 [37]	SkM* [29]
$f_{\rm opt}$	0.964	0.923	0.903	0.954	0.937	0.915	0.903	0.927
$\chi^2_{\rm log,m}$	0.0189	0.0095	0.0068	0.0065	0.0063	0.0063	0.0062	0.0061

4. Conclusion and discussion

In this work, the fusion barriers of a large number of fusion reactions have been studied systematically. We have proposed a method to obtain the distribution of the fusion barrier heights, which is the superposition of a set of Gaussian functions with parameters determined by the measured fusion excitation function. The advantage of the method is that in contrast to the second derivative method less data points are needed to achieve a similar result, and thus a lot of experimental data obtained before with a little lower precision can also be analyzed for obtaining helpful information about the fusion barriers. The main characteristics of the fusion barrier distributions, such as the mean barrier heights, full widths at half maximum (FWHM) and especially the diffusenesses at both sides of the distributions can be determined more precisely than those of the single Gaussian fitting approach [12]. The left side diffuseness of the distribution has a close relation with the enhancement and suppression of fusion cross sections at sub-barrier fusion. The mean barrier heights determined from the measured data with the method given in this work are compared with the parametrization of the empirical barrier distributions proposed in [14] for a total of 120 fusion reactions. It is found that the global features of the empirical barrier distributions are in good agreement with those determined from the experimental data for most reactions.

For understanding the physics behind the extracted and the empirical fusion barrier distributions, the influence of the static deformation and the deformation due to the excitation of the reaction partners on the reduction of the fusion barriers has been systematically investigated for a series of reactions induced by ^{16}O. We find that the reduction of the fusion barriers due to the static deformation in the fusion reactions with deformed nuclei and that due to the deformation caused by the excitation in the reactions with near-spherical nuclei are comparable. A barrier reduction factor is found to be about 5%. In addition, by searching for the optimal value of the reduction factor of the empirical barrier distribution, we find that the nucleus–nucleus interaction potentials calculated with the common used Skyrme interactions can give a good description of the fusion cross sections at energies near and above the barriers.

Acknowledgments

This work is supported by Alexander von Humboldt Foundation and National Natural Science Foundation of China, Nos 10235030, 10235020.

References

[1] Wong C Y 1973 *Rev. Lett.* **31** 766
[2] Keller J, Schmidt K H, Hessberger F P, Muenzenberg G and Reisdorf W 1986 *Nucl. Phys.* A **452** 173
[3] Rowley N, Satchler G R and Stelson P H 1991 *Phys. Lett.* B **254** 25
[4] Leigh J R, Dasgupta M and Hinde D J 1995 *Phys. Rev.* C **52** 3151
[5] Timmers H *et al* 1997 *J. Phys. G: Nucl. Part. Phys.* **23** 1175
Timmers H *et al* 1998 *Nucl. Phys.* A **633** 421

[6] Puri R K and Gupta R K 1992 *Phys. Rev.* C **45** 1837
[7] Hagino K, Rowley N and Kruppa A T 1999 *Comput. Phys. Commun.* **123** 143
[8] Newton J O *et al* 2004 *Phys. Rev.* C **70** 024605
[9] Simenel C, Chomaz Ph and France de G 2004 *Phys. Rev. Lett.* **93** 102701
[10] Umar A S and Oberacker V E 2006 *Phys. Rev.* C **74** 021601
[11] Maruhn J A, Reinhard P G, Stevenson P D and Strayer M R 2006 *Phys. Rev.* C **74** 027601
[12] Siwek-Wilczynska K and Wilczynski J 2004 *Phys. Rev.* C **69** 024611
[13] Stefanini A M, Trotta M and Behera B R 2005 *Eur. Phys. J.* A **23** 473
[14] Liu M, Wang N, Li Z, Wu X and Zhao E 2006 *Nucl. Phys.* A **768** 80 , and the references therein
[15] Stelson P H 1988 *Phys. Lett.* B **205** 190
[16] Morton C R, Berriman A C and Dasgupta M 1999 *Phys. Rev.* C **60** 044608
[17] Newton J O, Morton C R and Dasgupta M 2001 *Phys. Rev.* C **64** 64608
[18] Mukherjee A, Dasgupta M and Hinde D J 2002 *Phys. Rev.* C **66** 34607
[19] Stefanini A M, Ackermann D and Corradi L 1995 *Phys. Rev.* C **52** 1727
[20] Stefanini A M *et al* 1997 *J. Phys. G: Nucl. Part. Phys.* **23** 1401
[21] Trotta M *et al* 2005 *Eur. Phys. J.* A **25** 615
[22] Hinde D J, Berriman A C and Dasgupta M 1999 *Phys. Rev.* C **60** 054602
[23] Zhang H *et al* 2002 *J. Nucl. Radiochem. Sci.* **3** 99
[24] Stefanini A M *et al* 2000 *Phys. Rev.* C **62** 14601
[25] Sonzogni A A *et al* 1998 *Phys. Rev.* C **57** 722
[26] Trotta M, Stefanini A M and Corradi L 2001 *Phys. Rev.* C **65** 011601
[27] Zagrebaev V I 2001 *Phys. Rev.* C **64** 034606
[28] Brack M, Guet C and Hakanson H B 1985 *Phys. Rep.* **123** 275
[29] Bartel J, Quentin P h, Brack M, Guet C and Hakansson H B 1982 *Nucl. Phys.* A **386** 79
[30] Dasgupta M *et al* 1998 *Annu. Rev. Nucl. Part. Sci.* **48** 401
[31] Moller P, Nix J R, Myers W D and Swiatecki W J 1995 *At. Data and Nucl. Data Tables* **59** 185
[32] Gontchar I I *et al* 2004 *Phys. Rev.* C **69** 024610
[33] Myers W D and Swiatecki W J 2000 *Phys. Rev.* C **62** 044610
[34] Beiner M, Flocard H, Van Nguyen Giai and Quentin P 1975 *Nucl. Phys.* A **238** 29
[35] Dobaczewski J, Flocard H and Treiner J 1984 *Nucl. Phys.* A **422** 103
[36] Chabanat E *et al* 1997 *Nucl. Phys.* A **627** 710
Chabanat E *et al* 1997 *Nucl. Phys.* A **635** 231
[37] Samyn M, Goriely S, Bender M and Pearson J M 2004 *Phys. Rev.* C **70** 044309